Searchlight and Doppler Effects in the Visualization of Special Relativity: A Corrected Derivation of the Transformation of Radiance

DANIEL WEISKOPF, UTE KRAUS and HANNS RUDER
University of Tübingen

We demonstrate that a photo-realistic image of a rapidly moving object is dominated by the searchlight and Doppler effects. Using a photon-counting technique, we derive expressions for the relativistic transformation of radiance. We show how to incorporate the Doppler and searchlight effects in the two common techniques of special relativistic visualization, namely ray tracing and polygon rendering. Most authors consider geometrical appearance only and neglect relativistic effects on the lighting model. Chang et al. [1996] present an incorrect derivation of the searchlight effect, which we compare to our results. Some examples are given to show the results of image synthesis with relativistic effects taken into account.

Categories and Subject Descriptors: I.3.7 [**Three-Dimensional Graphics and Realism**]: Color, shading, shadowing, and texture; J.2 [**Physical Sciences and Engineering**]: Physics

General Terms: Algorithms, Theory

Additional Key Words and Phrases: Aberration of light, Doppler effect, illumination, Lorentz transformation, searchlight effect, special relativity

1. INTRODUCTION

Einstein's Theory of Special Relativity is widely regarded as a difficult and hardly comprehensible theory. One important reason for this is that the properties of space, time, and light in relativistic physics are totally different from those in classical, Newtonian physics. In many respects, they are contrary to human experience and everyday perception, which is based on low velocities.

Mankind is limited to very low velocities compared to the speed of light. For example, the speed of light is a million times faster than the speed of an airplane and 40,000 times faster than the speed at which the Space Shuttle orbits the Earth.

Address: Theoretical Astrophysics, University of Tübingen, Auf der Morgenstelle 10, D-72076 Tübingen, Germany

Permission to make digital or hard copies of part or all of this work for personal or classroom use is granted without fee provided that copies are not made or distributed for profit or direct commercial advantage and that copies show this notice on the first page or initial screen of a display along with the full citation. Copyrights for components of this work owned by others than ACM must be honored. Abstracting with credit is permitted. To copy otherwise, to republish, to post on servers, to redistribute to lists, or to use any component of this work in other works, requires prior specific permission and/or a fee. Permissions may be requested from Publications Dept, ACM Inc., 1515 Broadway, New York, NY 10036 USA, fax +1 (212) 869-0481, or `permissions@acm.org`.

Even in the long term, there is no hope of achieving velocities comparable to the speed of light. Therefore, computer simulations are the only means of visually exploring the realm of special relativity and can thus help the intuition of physicists.

The visual appearance of rapidly moving objects shows intriguing effects of special relativity. Apart from a previously disregarded article by Lampa [1924] about the invisibility of the Lorentz contraction, the first solutions to this problem were given by Penrose [1959] and Terrell [1959]. Various aspects were discussed by Weisskopf [1960], Boas [1961], Scott and Viner [1965], Scott and van Driel [1970], and Kraus [1999].

Hsiung and Dunn [1989] were the first to use advanced visualization techniques for image shading of fast moving objects. They propose an extension of normal three-dimensional ray tracing. Hsiung and Thibadeau [1990] and Hsiung et al. [1990] add the visualization of the Doppler effect. Hsiung, Thibadeau, and Wu [1990] and Gekelman et al. [1991] describe a polygon rendering approach which is based on the apparent shapes of objects as seen by a relativistic observer. Polygon rendering was also used as a basis for a virtual environment for special relativity [Rau et al. 1998; Weiskopf 1999].

Most authors concentrate their efforts on geometrical appearance and, apart from the Doppler effect, neglect relativistic effects on the lighting model. Chang et al. [1996], however, present a complete description of image shading which takes into account relativistic effects. We agree with most parts of their article, but we would like to correct their derivation of the relativistic transformation of radiance. We will show how the correct transformation of radiance fits in their shading process. The combination of Chang et al.'s work and this article gives a comprehensive presentation of special relativistic rendering.

We will demonstrate that a photo-realistic image would be dominated by the searchlight and Doppler effects, which are greatly underestimated when one is viewing the examples given by Chang et al. The Doppler effect causes a shift in wavelength of the incoming light, which results in a change of color. The searchlight effect increases the apparent brightness of the objects ahead when the observer is approaching these objects at high velocity. Amongst others, the Doppler effect, the relativistic aberration of light, and the time dilation contribute to the searchlight effect.

2. DERIVATION OF THE TRANSFORMATIONS

2.1 The Transformation of Radiance

The following derivation of the searchlight effect is based on a photon-counting technique. A similar approach can be found in articles by Peebles and Wilkinson [1968], McKinley [1979, 1980], and Kraus [1999].

Let us consider two inertial frames of reference, S and S', with S' moving with velocity v along the z axis of S. Suppose the observer O is at rest relative to S and the observer O' is moving with speed v along the z axis of S. The usual Lorentz transformation along the z axis connects frames S and S'.

In reference frame S, consider a photon with circular frequency ω, wavelength λ, energy E, and wave vector $\vec{k} = (\omega \sin\theta\cos\phi, \omega \sin\theta \sin\phi, \omega\cos\theta)/c$ with spherical coordinates θ and ϕ, as shown in Fig. 1.

In frame S', the circular frequency is ω', the wavelength is λ', the energy is E', and the wave vector is $\vec{k'} = (\omega' \sin\theta' \cos\phi', \omega' \sin\theta' \sin\phi', \omega' \cos\theta')/c$. The expressions for the Doppler effect and the aberration connect these two representations, cf. [McKinley 1979; Møller 1972]:

$$\lambda' = \lambda\, D, \tag{1}$$

$$\omega' = \omega/D, \tag{2}$$

$$E' = E/D, \tag{3}$$

$$\cos\theta' = \frac{\cos\theta - \beta}{1 - \beta\cos\theta}, \tag{4}$$

$$\phi' = \phi, \tag{5}$$

$$D = \frac{1}{\gamma(1 - \beta\cos\theta)}, \tag{6}$$

where D is the Doppler factor, $\gamma = 1/\sqrt{1-\beta^2}$, $\beta = v/c$, and c is the speed of light.

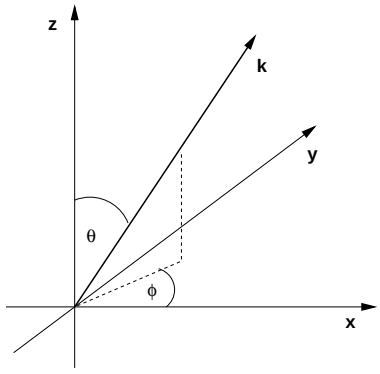

Fig. 1. A photon with wave vector $\vec{k}$.

Radiance is the radiant power per unit of foreshortened area emitted into a unit solid angle. A detector at rest in S will measure the energy dependent radiance

$$L_E(\theta,\phi) = \frac{d\Phi}{dE\, dA_\perp\, d\Omega},$$

where Φ is the radiant power or radiant flux, E is the energy, $d\Omega$ is the solid angle, and $dA_\perp$ is the area dA of the detector projected along the radiation direction (θ,ϕ). The radiant flux Φ is the radiant energy per unit time. Accordingly, the wavelength dependent radiance is

$$L_\lambda(\theta,\phi) = \frac{d\Phi}{d\lambda\, dA_\perp\, d\Omega}, \tag{7}$$

with the wavelength λ.

In reference frame S, consider a group of photons, dN in number, with energies between E and $E + dE$ and propagation directions in the element of solid angle $d\Omega$

around (θ, ϕ). Here, the energy dependent radiance is

$$L_E(\theta, \phi) = \frac{dN\,E}{dE\,dA_\perp\,d\Omega\,dt},$$

or

$$dN = \frac{L_E(\theta, \phi)}{E}\,dE\,dA_\perp\,d\Omega\,dt.$$

We choose the area dA to be perpendicular to the z axis so that

$$dA_\perp = dA\cos\theta.$$

The z component of the velocity of the photons is $c\cos\theta$. The photons passing dA between time t_0 and time $t_0 + dt$ are contained in the shaded volume dV in Fig. 2:

$$dV = dA\,dt\,c\cos\theta.$$

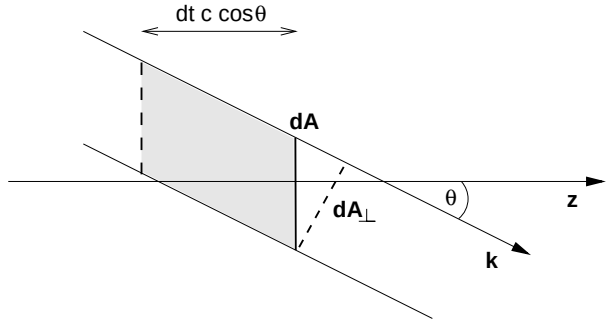

Fig. 2. Photons with propagation direction along the wave vector $\vec{k}$. The area of the detector is denoted dA and is perpendicular to the z axis, $dA_\perp$ is the projection of dA along the radiation direction. The shaded volume dV contains the photons passing dA between time t_0 and time $t_0 + dt$.

Consider another area $d\tilde{A}$ having the same size and orientation as dA. Still in reference frame S, suppose $d\tilde{A}$ is moving with velocity v along the z axis. The photons passing $d\tilde{A}$ between t_0 and $t_0 + dt$ are contained in the shaded volume in Fig. 3:

$$d\tilde{V} = dA\,dt\,(c\cos\theta - v) = \frac{\cos\theta - \beta}{\cos\theta}dV.$$

The ratio of the number of photons passing $d\tilde{A}$ in the time interval dt and the number of photons passing dA is the same as the ratio of the volume $d\tilde{V}$ and the volume dV:

$$d\tilde{N} = \frac{L_E(\theta, \phi)}{E}\,dE\,d\Omega\,dt\,\cos\theta\,d\tilde{A}\,\frac{\cos\theta - \beta}{\cos\theta}. \tag{8}$$

Now consider the same situation in reference frame S'. The area $d\tilde{A}$ is at rest in S'. The time interval is

$$dt' = dt/\gamma. \tag{9}$$

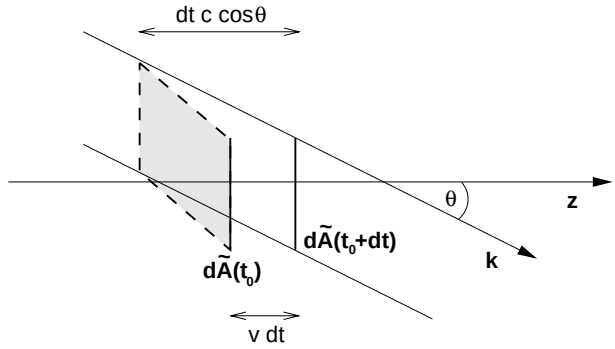

Fig. 3. Photons with propagation direction along the wave vector $\vec{k}$. The area $d\tilde{A}$ is moving with velocity v along the z axis. The shaded volume $d\tilde{V}$ contains the photons passing $d\tilde{A}$ between t_0 and $t_0 + dt$.

The number of photons counted does not depend on the frame of reference, i.e.

$$d\tilde{N} = d\tilde{N}' = \frac{L'_{E'}(\theta', \phi')}{E'}\, dE'\, d\Omega'\, dt'\, \cos\theta'\, d\tilde{A}'. \tag{10}$$

From Eqs. (8) and (10) we obtain

$$\frac{L_E(\theta, \phi)}{L'_{E'}(\theta', \phi')} = \frac{E}{E'}\frac{dE'}{dE}\frac{d\Omega'}{d\Omega}\frac{dt'}{dt}\frac{\cos\theta'}{\cos\theta - \beta}\frac{d\tilde{A}'}{d\tilde{A}}. \tag{11}$$

Since the area $d\tilde{A}$ is perpendicular to the separating velocity, it is not changed by Lorentz transformations:

$$d\tilde{A}' = d\tilde{A}. \tag{12}$$

With Eqs. (4) and (5), the transformed solid angle is

$$\frac{d\Omega'}{d\Omega} = \frac{\sin\theta'}{\sin\theta}\frac{d\theta'}{d\theta} = \frac{d(\cos\theta')}{d(\cos\theta)} = \frac{1}{\gamma^2(1 - \beta\cos\theta)^2} = D^2. \tag{13}$$

Using Eqs. (3), (4), (9), (12), (13), and (11), we obtain

$$\frac{L_E(\theta, \phi)}{L'_{E'}(\theta, \phi)} = D^3 = \frac{E^3}{E'^3}.$$

With the relation between energy and wavelength,

$$\lambda = \frac{hc}{E}, \qquad d\lambda = -\frac{hc}{E^2}dE,$$

and with

$$L_\lambda(\theta, \phi)\, |d\lambda| = L_E(\theta, \phi)\, |dE|,$$

we get

$$L_\lambda(\theta, \phi) = L_E(\theta, \phi)\frac{E^2}{hc}.$$

Ultimately, then, the transformation expression for the wavelength dependent radiance is

$$\frac{L_\lambda(\theta,\phi)}{L'_{\lambda'}(\theta',\phi')} = D^5. \tag{14}$$

From this equation the transformation law for the following integrated quantity is easily obtained. With the use of Eq. (1), the transformed radiance is

$$L(\theta,\phi) = \int_0^\infty L_\lambda(\theta,\phi)\,d\lambda = D^4 \int_0^\infty L'_{\lambda'}(\theta',\phi')\,d\lambda' = D^4 L'(\theta',\phi'). \tag{15}$$

2.2 Incident Irradiance from a Point Light Source

The measure for radiant power leaving a point light source in an element of solid angle $d\Omega$ and in a wavelength interval is called the wavelength dependent intensity I_λ:

$$I_\lambda = \frac{d\Phi}{d\Omega\,d\lambda}. \tag{16}$$

The wavelength dependent irradiance E^i_λ is the radiant power per unit area in a wavelength interval:

$$E^i_\lambda = \frac{d\Phi}{dA\,d\lambda}. \tag{17}$$

For a surface patch on the object, the wavelength dependent irradiance $E^{i'}_{\lambda'}$ coming from a moving point light source is

$$E^{i'}_{\lambda'} = \frac{1}{D^5}\frac{\cos\alpha'}{r'^2} I_\lambda, \tag{18}$$

with the angle α' between the normal vector to the surface and the direction of the incident photons, and with the apparent distance r' of the light source from the surface patch. These quantities are measured in the reference frame of the object, whereas the wavelength dependent intensity I_λ is measured in the reference frame of the light source. Accordingly, the integrated, wavelength independent irradiance is

$$E^{i'} = \frac{1}{D^4}\frac{\cos\alpha'}{r'^2} I. \tag{19}$$

The derivation of these equations is presented in the Appendix. Observe that, for an isotropic point source in one frame of reference, we get an anisotropic source in the other frame of reference due to the implicit angle dependency in the Doppler factor D.

3. COMPARISON WITH DERIVATION BY CHANG ET AL.

Chang et al. [1996] present a complete treatment of relativistic image shading, which contains apparent geometry, the searchlight and Doppler effects, and a detailed description of the shading process. However, their derivation of the transformation properties of radiance is based on wrong interpretations of the Theory of Special Relativity and leads to a tremendous divergence from our correct results presented above.

Chang et al. derive their expressions based on the assumption that the same amount of radiant power is emitted from a surface patch on the object and the corresponding surface patch on the apparent surface. Ensuingly, they compute the relation between the area of the surface patch on the object and the area of the corresponding surface patch on the apparent surface, as well as the relation between the respective normal vectors. They treat the apparent surface as an object at rest with respect to the observer.

Their derivation is not correct because of the following reasons:

Radiant power depends on time intervals and on the energy of photons, both of which are subject to Lorentz transformations. These transformations are missing in Chang et al.'s work.

The observer is moving with respect to the surface patch of the object. Approaching the object, the observer's detector sweeps up photons so that the rate at which radiant energy is received is increased by the observer's motion. This increase is absent for radiation from the apparent surface, which is stationary in the observer's rest frame. Chang et al. ignore this effect as well.

Chang et al.'s transformation of solid angle in their Eq. (36) is not correct. The mistake is due to their calculation of the partial derivatives $\partial\Theta'/\partial\Theta$, $\partial\Theta'/\partial\Phi$, $\partial\Phi'/\partial\Theta$ and $\partial\Phi'/\partial\Phi$ with the use of their Eq. (31) for the transformation of the direction of the light ray. Their Eq. (31) is valid for the special case of polar angle $\Theta = \pi/2$ only and cannot be used to calculate partial derivatives.

Both wavelength and wavelength intervals are subject to Lorentz transformations. When calculating the radiance per wavelength interval in their Eq. (39) from Eq. (38) for the radiance, Chang et al. apply the Lorentz transformation to the wavelength, but not to the wavelength interval.

Ultimately, they end up with a factor of D in the transformation of radiance in their Eq. (38) and in the transformation of wavelength dependent radiance in their Eq. (39), which differs from the correct result by a factor of D^3 and D^4, respectively. Similarly, their calculation of irradiance in their Eq. (46) and of wavelength dependent irradiance in their Eq. (47) differs from the correct result by the same factor of D^3 and D^4, respectively.

4. THE SHADING PROCESS

The searchlight and Doppler effects can readily be incorporated in the two common techniques of special relativistic visualization, which are ray tracing and polygon rendering.

Relativistic ray tracing as described by Hsiung and Dunn [1989] is an extension of normal three-dimensional ray tracing. The ray starting at the eye point and intersecting the viewing plane is transformed according to special relativity, i.e. the direction of light is turned due to relativistic aberration. At this point, the transformed properties of light can be included by calculating the transformed radiance as well as the transformed wavelength.

In this framework, it is not sufficient to consider only three tristimulus values, such as RGB, but the wavelength dependent energy distribution of light has to be taken into account. The spectral energy distribution has to be known over an extensive range so that the Doppler-shifted energy distribution can be calculated for wavelengths in the visible range. For final image synthesis, the tristimulus values

can easily be obtained from the wavelength dependent radiance that gets to the eye point.

Relativistic polygon rendering is based on the apparent shapes of objects with respect to the observer. In full detail, the shading process is described by Chang et al. In this process, merely the expressions for irradiance in step (2)(d)(iv) and for the transformation of radiance in step (2)(f) have to be replaced by our Eqs. (18) and (14), respectively. The Doppler factor in Eq. (18) depends on the direction of the photons reaching the object and on the relative velocity of the frame of the point light source and of the frame of the object, whereas the Doppler factor in Eq. (14) depends on the direction of the photons reaching the observer and on the relative velocity of the frame of the object and of the frame of the observer.

5. EXAMPLES

The appearance of a scene similar to Chang et al.'s STREET in Figs. 4–7 shows the tremendous effects of the transformation of radiance on image synthesis. These pictures visualize the apparent geometry and the radiance transformation, but neglect color changes due to the Doppler effect. Since the spectral energy distribution of the light reflected by the objects of the STREET is unknown, we only show grey-scale images that take into account the total energy of the whole spectral energy distribution. In this case, Eq. (15) is applied. If we used a speed as high as Chang et al.'s $0.99c$, we would not be able to display the high intensities in Fig. 7 properly. Therefore, we choose a velocity of $0.8c$. These images were generated by using the ray tracing method described above. The relativistic extensions are implemented into *RayViS* [Gröne 1996], a normal three-dimensional ray tracing program.

Figs. 8 and 9 show the appearance of the sun moving at a speed of $0.5c$ to illustrate color changes due to relativistic lighting. For the production of these images we used the polygon rendering technique described above. A detailed presentation of the rendering software can be found in our previous work [Rau et al. 1998; Weiskopf 1999].

6. CONCLUSION

We have demonstrated that, aside from the apparent geometry, the searchlight and Doppler effects play dominant roles in special relativistic visualization. Ray tracing and polygon rendering, two standard techniques in computer graphics, can easily be modified and extended to take into account the searchlight and Doppler effects.

The transformation of radiance could serve as an important element in even more sophisticated shading algorithms in order to generate photo-realistic and physically correct images of fast moving objects. For example, radiosity could be extended to visualize relativistic flights through stationary scenes.

ACKNOWLEDGMENTS

This work was supported by the Deutsche Forschungsgemeinschaft (DFG) and is part of the project D4 within the Sonderforschungsbereich 382.

Fig. 4. Original appearance of the street

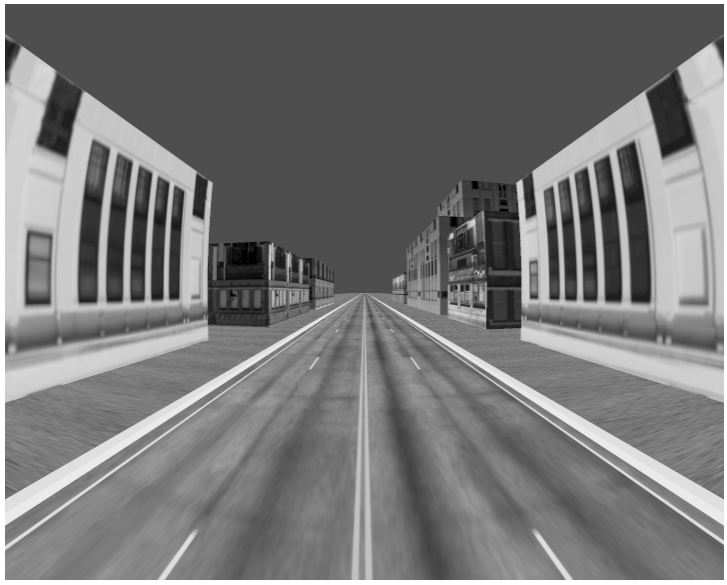

Fig. 5. Appearance of the street with respect to a moving observer. The viewer is rushing into the street with a speed of $0.8c$. The light sources are at rest in the coordinate system of the street. The searchlight and Doppler effects are ignored.

Fig. 6. Visualization of the searchlight effect based on the incorrect derivation by Chang et al. The viewer is rushing into the street with a speed of $0.8c$. The light sources are at rest in the coordinate system of the street.

Fig. 7. Visualization of the searchlight effect based on the correct Eq. (15) for the transformation of radiance. The difference to Fig. 6 is significant. The viewer is rushing into the street with a speed of $0.8c$. The light sources are at rest in the coordinate system of the street.

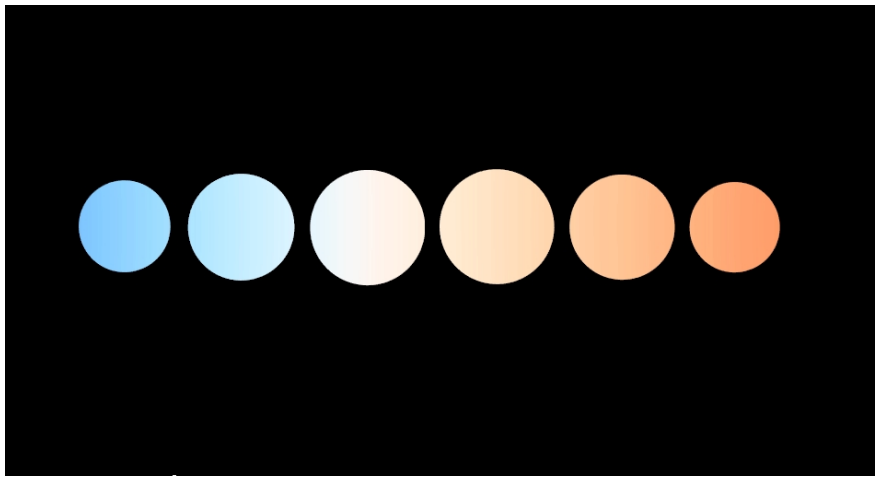

Fig. 8. Visualization of the Doppler effect only, in the sense that the Doppler-shifted spectral energy distribution is shown with no further transformations. The sun is passing by with a speed of $0.5c$. The sun is the only light source and is emitting blackbody radiation with a temperature of 5762 Kelvin.

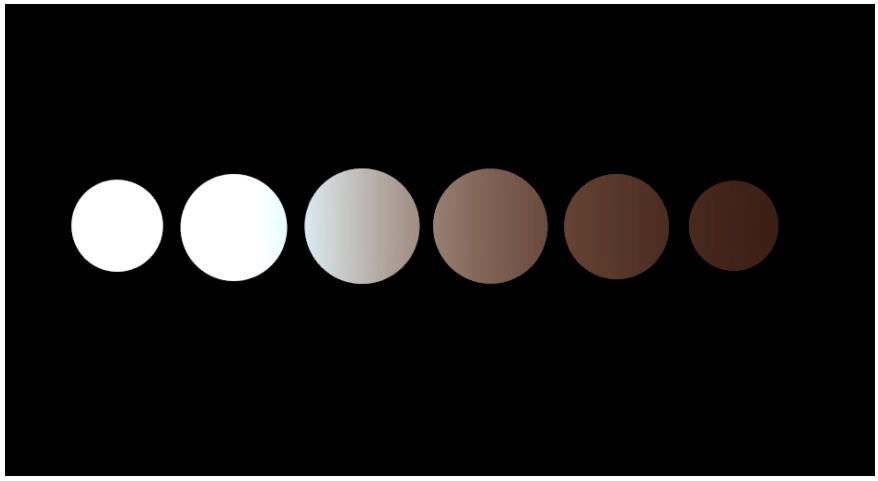

Fig. 9. Visualization of the searchlight and Doppler effects based on Eq. (14). The sun is passing by with a speed of $0.5c$. The sun is the only light source and is emitting blackbody radiation with a temperature of 5762 Kelvin.

APPENDIX

A. INCIDENT IRRADIANCE

In this Appendix the derivation of Eqs. (18) and (19) is presented.

First, consider a finite light source which is at rest in frame S. With Eq. (7), the radiant flux emitted by the light source can be obtained in terms of the wavelength dependent radiance:

$$d\Phi = L_\lambda \, dA_\perp^{light} \, d\Omega^{obj} \, d\lambda, \tag{20}$$

where $dA_\perp^{light}$ is the area of the projected surface patch of the light source and $d\Omega^{obj}$ is the solid angle of the illuminated surface patch of the object as seen from the position of the light source.

Now consider the same situation in frame S' in which the object is at rest. The radiant flux on the surface patch of the object is

$$d\Phi' = L'_{\lambda'} dA_\perp^{obj'} \, d\Omega^{light'} \, d\lambda', \tag{21}$$

with the projected area $dA_\perp^{obj'}$ on the object and the solid angle $d\Omega^{light'}$ of the surface patch of the light source as seen from the position of the object. Using Eqs. (14) and (21), we obtain

$$d\Phi' = \frac{1}{D^5} L_\lambda dA_\perp^{obj'} \, d\Omega^{light'} \, d\lambda'.$$

With the definition in Eq. (17), the incident irradiance emitted from the small solid angle $d\Omega^{light'}$ onto the surface patch of the object is

$$dE_{\lambda'}^{i'} = \frac{d\Phi'}{dA^{obj'} \, d\lambda'} = \frac{L_\lambda}{D^5} \frac{dA_\perp^{obj'}}{dA^{obj'}} d\Omega^{light'}. \tag{22}$$

The area $dA^{obj'}$ of the surface patch is related to the projected area $dA_\perp^{obj'}$ by

$$dA_\perp^{obj'} = dA^{obj'} \cos\alpha', \tag{23}$$

with the angle α' between the surface normal and the incident light.

With Eq. (13), the solid angle $d\Omega^{light'}$ is transformed into the frame S of the light source. Furthermore, $d\Omega^{light'}$ is expressed in terms of the projected area on the light source and of the distance between the light source and the surface patch, as shown in Fig. 10:

$$d\Omega^{light'} = D^2 \, d\Omega^{light} = D^2 \, \frac{dA_\perp^{light}}{r^2} = dA_\perp^{light} \left(\frac{D}{r}\right)^2. \tag{24}$$

The light-like connection of the emission event at the light source and the absorption event at the object has the same direction as the wave vector that describes the photons. Therefore, the distance r is transformed in the same way as the circular frequency ω, see Eq. (2). By following this reasoning or by explicit Lorentz transformation of the separating vector between the emission event and the absorption event, we get:

$$r' = r/D. \tag{25}$$

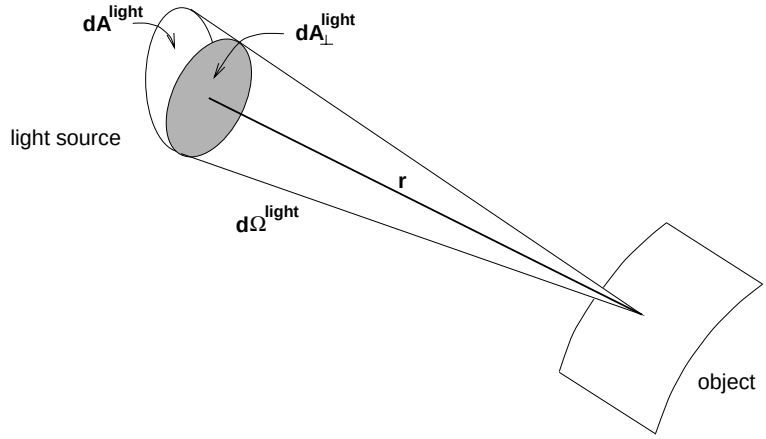

Fig. 10. Geometry of the surface patch of the light source in its rest frame S. The solid angle is given by $d\Omega^{light} = dA_{\perp}^{light}/r^2$. The distance between the light source at emission time and the surface patch of the object at absorption time is denoted r.

Using Eqs. (22), (23), (24), and (25), we obtain the incident wavelength dependent irradiance originating from a small area of the light source:

$$dE_{\lambda'}^{i'} = \frac{1}{D^5}\frac{\cos\alpha'}{r'^2} L_\lambda \, dA_{\perp}^{light}.$$

By integrating over the area of the whole light source, we get the wavelength dependent irradiance produced by this finite light source:

$$E_{\lambda'}^{i'} = \int \frac{1}{D^5}\frac{\cos\alpha'}{r'^2} L_\lambda \, dA_{\perp}^{light}. \tag{26}$$

Now, consider a very small, yet finite light source described by its wavelength dependent intensity I_λ. With Eqs. (16) and (20), the wavelength dependent radiance and the wavelength dependent intensity from the area $dA_{\perp}^{light}$ are related by

$$dI_\lambda = L_\lambda \, dA_{\perp}^{light}. \tag{27}$$

With Eq. (26) and after integrating over the area of the small light source, we find the wavelength dependent irradiance on the object:

$$E_{\lambda'}^{i'} = \int \frac{1}{D^5}\frac{\cos\alpha'}{r'^2} L_\lambda \, dA_{\perp}^{light} = \frac{1}{D^5}\frac{\cos\alpha'}{r'^2} \int L_\lambda \, dA_{\perp}^{light} = \frac{1}{D^5}\frac{\cos\alpha'}{r'^2} I_\lambda.$$

This equation holds even for the limit of an infinitesimal light source. Therefore, we obtain the wavelength dependent irradiance due to a point light source:

$$E_{\lambda'}^{i'} = \frac{1}{D^5}\frac{\cos\alpha'}{r'^2} I_\lambda.$$

Accordingly, the irradiance is

$$E^{i'} = \frac{1}{D^4}\frac{\cos\alpha'}{r'^2} I,$$

where I is the intensity of the light source.

REFERENCES

Boas, M. L. 1961. Apparent shape of large objects at relativistic speeds. *American Journal of Physics 29*, 5 (May), 283–286.

Chang, M.-C., Lai, F., and Chen, W.-C. 1996. Image shading taking into account relativistic effects. *ACM Transactions on Graphics 15*, 4 (Oct.), 265–300.

Gekelman, W., Maggs, J., and Xu, L. 1991. Real-time relativity. *Computers in Physics 5*, 4 (July/Aug.), 372–385.

Gröne, A. 1996. *Entwurf eines objektorientierten Visualisierungssystems auf der Basis von Raytracing*. Ph. D. thesis, University of Tübingen, Germany. In German.

Hsiung, P.-K. and Dunn, R. H. P. 1989. Visualizing relativistic effects in spacetime. In *Proceedings of Supercomputing '89 Conference* (1989), pp. 597–606.

Hsiung, P.-K. and Thibadeau, R. H. 1990. Spacetime visualization of relativistic effects. In *Proceedings of the 1990 ACM Eighteenth Annual Computer Science Conference* (Washington, DC, Feb. 1990), pp. 236–43.

Hsiung, P.-K., Thibadeau, R. H., Cox, C. B., Dunn, R. H. P., Wu, M., and Olbrich, P. A. 1990. Wide-band relativistic doppler effect visualization. In *Proceedings of the Visualization 90 Conference* (Oct. 1990), pp. 83–92.

Hsiung, P.-K., Thibadeau, R. H., and Wu, M. 1990. T-buffer: Fast visualization of relativistic effects in spacetime. *Computer Graphics (1990 Symposium on Interactive 3D Graphics) 24*, 2 (March), 83–88.

Kraus, U. 1999. Brightness and colour of rapidly moving objects: The visual appearance of a large sphere revisited. To appear in the *American Journal of Physics*.

Lampa, A. 1924. Wie erscheint nach der Relativitätstheorie ein bewegter Stab einem ruhenden Beobachter? *Zeitschrift für Physik 27*, 138–148. In German.

McKinley, J. M. 1979. Relativistic transformations of light power. *American Journal of Physics 47*, 7 (July), 602–605.

McKinley, J. M. 1980. Relativistic transformation of solid angle. *American Journal of Physics 48*, 8 (Aug.), 612–614.

Møller, C. 1972. *The Theory of Relativity* (Second ed.). Clarendon Press, Oxford.

Peebles, P. J. E. and Wilkinson, D. T. 1968. Comment on the anisotropy of the primeval fireball. *Physical Review 174*, 5 (Oct.), 2168.

Penrose, R. 1959. The apparent shape of a relativistically moving sphere. *Proceedings of the Cambridge Philosophical Society 55*, 137–139.

Rau, R. T., Weiskopf, D., and Ruder, H. 1998. Special relativity in virtual reality. In H.-C. Hege and K. Polthier Eds., *Mathematical Visualization*, pp. 269–279. Heidelberg: Springer Verlag.

Scott, G. D. and van Driel, H. J. 1970. Geometrical appearances at relativistic speeds. *American Journal of Physics 38*, 8 (Aug.), 971–977.

Scott, G. D. and Viner, R. R. 1965. The geomentrical appearence of large objects moving at relativistic speeds. *American Journal of Physics 33*, 7 (July), 534–536.

Terrell, J. 1959. Invisibility of the Lorentz contraction. *Physical Review 116*, 4 (Nov.), 1041–1045.

Weiskopf, D. 1999. An immersive virtual environment for special relativity. Report Nr. 108 (Jan.), SFB 382, University of Tübingen, Germany. http://www.uni-tuebingen.de/uni/opx/reports/weiskopf_108.ps.gz.

Weisskopf, V. F. 1960. The visual appearance of rapidly moving objects. *Physics Today 13*, 9, 24–27.